Exploring the Global Importance of Atmospheric Ammonia Oxidation

Sidhant J. Pai,* Colette L. Heald, and Jennifer G. Murphy*

Read Online

ACCESS | Metrics & More | Article Recommendations | Supporting Information

ABSTRACT: Ammonia (NH_3) is the dominant source of reduced nitrogen in the atmosphere, emitted primarily from agricultural activities. Current representations of NH_3 in global chemical transport models (CTMs) largely focus on the thermodynamics governing aerosol formation, ignoring the atmospheric oxidation of NH_3 with the hydroxyl (OH) radical since this process is slow and therefore assumed to not be significant. In this study, we incorporate an explicit mechanism to simulate this chemistry using the GEOS-Chem global CTM. While the inclusion of this pathway does not result in a meaningful impact on the global ammonia burden, with an average annual reduction of approximately 3%, the oxidation process leads to small but significant changes in key atmospheric species, particularly over the Indian subcontinent where surface concentrations of ozone (O_3), OH, and nitrate aerosol see reductions of over 5%. Our results also suggest that ammonia oxidation accounts for around 8% (and up to 16%) of the global anthropogenic nitrous oxide (N_2O) source, with important implications for climate models designed to accurately simulate the impact of changing agricultural emissions. We also conduct a suite of simulations using anthropogenic emission estimates from the representative concentration pathway (RCP) trajectories for 2100, which suggest that the atmospheric oxidation of NH_3 will become an increasingly important source of N_2O and NO_x under future emission scenarios, accounting for up to 21% of future N_2O emissions. Given the large uncertainties in the oxidation process, we use a sensitivity analysis to demonstrate the wide range in atmospheric response; our results support the need for further research to better constrain the reaction pathways and associated yields.

KEYWORDS: *ammonia, oxidation, agricultural emissions, climate, nitrate, NH_3, N_2O, NO_x*

1. INTRODUCTION

Ammonia (NH_3) is an important source of reactive nitrogen in the atmosphere and plays a vital role in the global nitrogen cycle. As the most abundant alkaline gas in the atmosphere, it has a significant influence on cloud pH and precipitation, impacting atmospheric chemistry at global and regional scales.[1] Ammonia is also an important regulator of natural water systems, and excessive deposition can result in algal blooms and degrade water quality, impacting sensitive ecosystems.[2,3] In the atmosphere, ammonia is a key precursor for secondary particulate formation, interacting with acidic species (such as sulfuric and nitric acids) to form sulfate, nitrate, and ammonium (SNA) aerosols along with various other salts. The resulting species account for a major fraction of the global secondary aerosol burden[4] and have a significant impact on global and regional climate.[5] Long-term exposure to elevated concentrations of such aerosols has also been linked to deleterious health outcomes by increasing the risks of respiratory and pulmonary diseases.[6,7]

Animal husbandry and fertilizer use for crops are by far the most abundant sources of atmospheric ammonia.[1,4,8] The
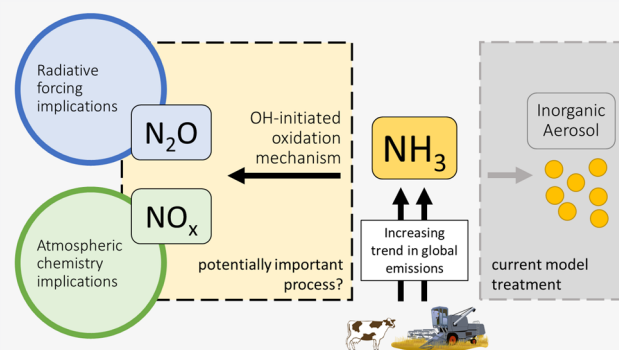
growing demand for synthetic fertilizer in the early 20th century resulted in the widespread implementation of the Haber−Bosch process to produce NH_3 at industrial scales, with studies estimating that close to half of the present-day global population depends on food produced using artificial nitrogen fertilizers.[9] Due to its volatile nature, the increase in ammonia fertilizer application has led to an increase in emissions of ammonia to the atmosphere. The expansion of intensive agriculture over the past century has thus increased global and regional atmospheric ammonia burdens well beyond natural levels.[9] This is particularly true in developing regions like South Asia, where NH_3 emissions from fertilizer use are estimated to have increased by an order of magnitude between 1961 and 2014.[10] With the growing global demand for food

Table 1. Rate Constants (cm^3 molecule^{-1} s^{-1}) for Representative Chemical Reactions Involved in the Ammonia Oxidation Process[a]

#	Reaction	Rate Constant	Rate Estimate at 298K (with uncertainty factors)	Reference
R_1	$NH_3 + OH \rightarrow NH_2 + H_2O$	$k_1 = 1.7 * 10^{-12} * e^{-\frac{710}{T}}$	1.6 (1.2) $* 10^{-13}$ cm^3 molecule^{-1} s^{-1}	C11 JPL-15-10
R_2	$NH_2 + O_3 \rightarrow NH_2O + O_2$	$k_2 = 4.3 * 10^{-12} * e^{-\frac{930}{T}}$	1.9 (3.0) $* 10^{-13}$ cm^3 molecule^{-1} s^{-1}	C27 JPL-15-10
R_{3a}	$NH_2 + NO_2 \rightarrow NH_2O + NO$	$k_{3a} = 2.0 * 10^{-11} * \left(\frac{T}{298}\right)^{-1.3} * (0.75)$	1.5 (1.6) $* 10^{-11}$ cm^3 molecule^{-1} s^{-1}	IUPAC Data Sheet NOx22. 2001
R_{3b}	$NH_2 + NO_2 \rightarrow N{=}N{=}O + H_2O$	$k_{3b} = 2.0 * 10^{-11} * \left(\frac{T}{298}\right)^{-1.3} * (0.25)$	0.5 (1.6) $* 10^{-11}$ cm^3 molecule^{-1} s^{-1}	
R_4	$NH_2 + NO \rightarrow N{\equiv}N + H_2O$	$k_4 = 4.0 * 10^{-12} * e^{\frac{450}{T}}$	1.8 (1.3) $* 10^{-11}$ cm^3 molecule^{-1} s^{-1}	C28 JPL-15-10
R_{5a}	$NH_2 + HO_2 \rightarrow NH_3 + O_2$	$k_{5a} = 3.4 * 10^{-11} * (0.85)$	2.9 (2.0) $* 10^{-11}$ cm^3 molecule^{-1} s^{-1}	C16 JPL-15-10 & Glarborg et al. 2021
R_{5b}	$NH_2 + HO_2 \rightarrow HNO + H_2O$	$k_{5b} = 3.4 * 10^{-11} * (0.01)$	3.4 (2.0) $* 10^{-13}$ cm^3 molecule^{-1} s^{-1}	C16 JPL-15-10 & Glarborg et al. 2021
R_{5c}	$NH_2 + HO_2 \rightarrow NH_2O + OH$	$k_{5c} = 3.4 * 10^{-11} * (0.14)$	4.8 (2.0) $* 10^{-12}$ cm^3 molecule^{-1} s^{-1}	C16 JPL-15-10 & Glarborg et al. 2021
R_6	$NH_2O + O_3 \rightarrow NH_2 + 2O_2$	$k_6 = 2.0 * 10^{-14}$	2.0 ($\pm$ 1.5) $* 10^{-14}$ cm^3 molecule^{-1} s^{-1}	Bulatov et al. 1980
R_7	$NH_2O + OH \rightarrow HNO + H_2O$	$k_7 = 1.8 * 10^{-10}$	1.8 (10) $* 10^{-10}$ cm^3 molecule^{-1} s^{-1}	Sun et al. 2001.
R_8	$HNO + O_2 \rightarrow NO + HO_2$	$k_8 = 3.65 * 10^{-14} * e^{-\frac{4600}{T}}$	7.2 (2) $* 10^{-21}$ cm^3 molecule^{-1} s^{-1}	Bryukov et al. 1993.

[a]Reaction R_8 is assumed to occur rapidly and is thus not explicitly simulated. Rate estimates are provided for each reaction at 298 K, with the uncertainty factor represented in red within parentheses in all cases except reaction R_6 where it represents an absolute error estimated by the study for the measurement at 296 K.

and animal products, ammonia emissions in these regions are expected to continue increasing well into the 21st century. This trend is in contrast to nitrogen oxide (NO_x) emissions, the other important source of reactive nitrogen in the atmosphere. With increasingly strict regulations, NO_x emissions are expected to stabilize and drop over the coming decades, a phenomenon already observed in Europe, North America, and China.[11] These opposing trends have resulted in a significant shift in the composition of atmospheric reactive nitrogen, with a move from oxidized nitrogen compounds toward the greater prevalence of reduced nitrogen compounds like NH_3.[12]

Model representations of NH_3 in global chemical transport models (CTMs) are relatively simple, focusing largely on the thermodynamics that govern the formation of ammonium aerosol and the deposition processes that dictate its loss. However, in addition to these processes, ammonia has also been shown to undergo oxidation initiated by the hydroxyl (OH) radical,[13] forming the short-lived amino radical (NH_2), which undergoes further oxidation with nitrogen oxide (NO), nitrogen dioxide (NO_2), ozone (O_3), or the hydroperoxyl radical (HO_2) to ultimately form molecular nitrogen (N_2), nitrous oxide (N_2O), or NO. The relative product yields are sensitive to the NO_x regime as well as to the relative abundance of ambient O_3. Kohlmann and Poppe[14] found that uncertainties in the kinetics of the amino radical led to a wide range of N_2O yields, from 10 to 43%. NH_2O is an intermediate product in this mechanism, arising from the reaction of NH_2 with NO_2, O_3, and HO_2, but its fate remains largely unstudied. Sun et al.[15] reported a large rate constant for the reaction of

NH_2O with OH, which favors the ultimate production of NO_x. Isomerization of NH_2O to NHOH, postulated by Bulatov et al.,[16] is also expected to have a significant impact on the NO_x yield from the oxidation of NH_3.

Chemical transport models have traditionally ignored ammonia oxidation from this mechanism due to the slow kinetics that govern the initial reaction of NH_3 with OH,[13] resulting in chemical lifetimes on the order of weeks. Other NH_3 loss mechanisms, such as uptake to particles and dry and wet deposition, operate on the order of around a day[17,18] and are thus expected to dominate the loss. While ammonia oxidation has been shown to not be a significant sink for global ammonia,[1,14,19−23] it is possible that this mechanism could result in the production of atmospherically significant levels of NO and N_2O over regions with elevated NH_3 burdens. N_2O is an important greenhouse gas, with a unit-mass radiative forcing that is almost 300 times greater than that from carbon dioxide over a 100 year time horizon.[24−26] However, it is emitted in comparatively small quantities, with recent global N_2O emissions estimated to be around 17.0 Tg N year^{-1}, of which 7.3 Tg N year^{-1} is anthropogenic.[27] Previous studies that have investigated the importance of atmospheric NH_3 oxidation have estimated a global N_2O source between 0.4 and 1.2 Tg N year^{-1} from this pathway,[1,14,20,21] suggesting that ammonia oxidation could indeed be a significant (up to 7%) contributor to global N_2O. Similarly, the fifth assessment report from the Intergovernmental Panel on Climate Change[24] suggests that atmospheric processes likely account for around 0.6 Tg N year^{-1} of N_2O production. However, there remain a

number of uncertainties surrounding the global relevance of this pathway.

The oxidation of ammonia also produces NO, with previous studies estimating a global NO_x source of around 0.9 Tg N year^{-1} from this mechanism.[19] When compared against a total NO_x source[28] of around 56 Tg N year^{-1}, the magnitude of NO production from this pathway appears relatively insignificant. However, some of the NO production from this mechanism occurs in remote regions and in the free troposphere (FT), where it could disproportionately influence oxidative chemistry and HO_x cycling,[29] similar to the impact of lightning NO_x.[30] Ammonia oxidation could thus impact numerous atmospheric species due to the tight coupling of the HO_x–NO_x–VOC–O_3 chemistry. SNA aerosol formation is also often limited by ammonia over polluted regions,[4] making it sensitive to the changes in ambient NH_3 concentrations. Despite this, there has been limited modeling to explicitly simulate the impact of ammonia oxidation,[1,14,19−23] with little investigation of the resulting spatial distributions of key atmospheric species such as O_3, NO, and SNA aerosols. Here, we revisit the role of ammonia oxidation in the atmosphere. We review reaction parameters from recent literature sources to create an updated representation of the oxidation process and incorporate an explicit oxidation mechanism within a global chemical transport model to better understand the impacts of this pathway on NH_3 and various other key atmospheric species. We also conduct a series of simulations using future NH_3 and NO_x emission estimates to assess whether the ammonia oxidation process might take on an increased salience in the coming decades.
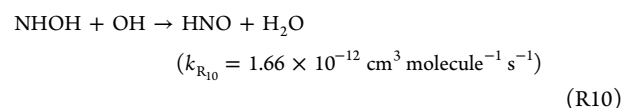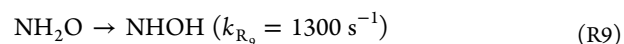
2. METHODS

To explore the global and regional implications of ammonia oxidation, we incorporate an ammonia oxidation mechanism into the standard chemical mechanism of the GEOS-Chem chemical transport model v12.1.1.[31] All model simulations are performed at a global horizontal resolution of 2° × 2.5°, with 47 vertical hybrid-sigma levels. The model is driven by the MERRA-2 assimilated meteorological product from the NASA Global Modeling and Assimilation Office (GMAO) with a chemistry time step of 20 min and a transport time step of 10 min, as recommended by Philip et al.[32]

The model includes a coupled treatment of HO_x–NO_x–VOC–O_3 chemistry[33−35] with integrated Cl−Br−I chemistry[36] and uses a standard bulk aerosol scheme with fixed log−normal modes. SNA thermodynamic partitioning is described using the ISORROPIA II model.[37] Production and loss diagnostics were created to track the chemical fluxes of NH_3, NO, N_2O, and N_2 resulting from the oxidation reactions. Table 1 provides an overview of the ammonia oxidation scheme explored here, with rate constants from the most recent JPL evaluations along with various other literature sources. While the reaction of NH_3 with OH is relatively well constrained, we note that there are large uncertainties in the rate constants for the subsequent reactions, with results from various studies differing by up to an order of magnitude. Similarly, the branching ratios that determine the fate of NH_2 when reacting with NO_2 are highly uncertain.[38] The reaction of NH_2 with HO_2 is also poorly constrained, as are the associated product yields.[39,40]

The model was run at a global domain for the year 2016 (preceded by a 6 month spin-up) and compared to a standard simulation without the oxidation mechanism over the same

time period to evaluate the relative importance of the ammonia oxidation pathway across a number of key atmospheric species. The standard simulation is referred to here as "Base". We use "AmOx" to refer to the simulation that includes the ammonia oxidation pathway. We also conduct two additional sensitivity simulations to evaluate the importance of various uncertainties in the mechanism. The simulation "MaxN$_2$O" is configured to provide an upper-bound estimate on N_2O production from this pathway. This is achieved by increasing the branching ratio of reaction R$_{3b}$ to 40%,[41] using lower-bound estimates for k_2, k_4, and k_7[15] and using an upper-bound estimate for k_6.[16] Conversely, the simulation "MaxNO$_x$" is configured to provide an upper-bound estimate on NO production. This is achieved by decreasing the reaction R$_{3b}$ branching ratio to 10%,[41] using an upper-bound estimate for k_2 and a lower-bound estimate for k_4.[41] In "MaxNO$_x$", we also implement an isomerization pathway[14,16,42] for the NH_2O produced in reactions R$_2$, R$_{3a}$,[14,16] and R$_{5c}$[39,40] described below, which is expected to favor additional NO production by limiting NH_2O recycling

$$NH_2O \rightarrow NHOH \ (k_{R_9} = 1300 \ s^{-1}) \tag{R9}$$

$$NHOH + OH \rightarrow HNO + H_2O$$
$$(k_{R_{10}} = 1.66 \times 10^{-12} \ cm^3 \ molecule^{-1} \ s^{-1}) \tag{R10}$$

Anthropogenic and agricultural emissions of ammonia and other species follow the Community Emissions Data System (CEDS) inventory.[43] These emissions are overwritten with regional inventories when available. NH_3 emissions over India, a region of particular interest, are from the MIX inventory.[44] Model NH_3 emissions for 2016 total 59.4 Tg N year^{-1}, of which 42.1 Tg N year^{-1} is from anthropogenic sources (including agricultural sources), 3 Tg N year^{-1} is from biomass burning, and 14.3 Tg N year^{-1} is from other natural sources. Nitrogen oxide emissions follow the same anthropogenic inventories and also include lightning,[45,46] soil,[47] and ship[48] sources. Model NO_x emissions for 2016 total 53 Tg N year^{-1}, of which 32.9 Tg N year^{-1} is from anthropogenic sources, 6.3 Tg N year^{-1} is from lightning, 6 Tg N year^{-1} is from biomass burning, and 7.8 Tg N year^{-1} is from soil sources. Biogenic emissions of volatile organic compounds are based on the coupled ecosystem emission model (Model of Emissions of Gases and Aerosols from Nature (MEGAN v2.1)).[49] Pyrogenic emissions are simulated from the GFED4s satellite-derived global fire emissions database.[50] Deposition losses are dictated by aerosol and gas dry deposition to surfaces based on a resistor-in-series scheme[51,52] and wet deposition from scavenging by rainfall and moist convective cloud updrafts.[53,54]

To explore the potential importance of the ammonia oxidation process under future emission scenarios, we conduct a series of simulations using both the base and AmOx model configurations. These simulations are driven by four different emission scenarios for the year 2100 that are generated in accordance with the representative concentration pathway (RCP) trajectories adopted by the fourth assessment report compiled by the Intergovernmental Panel on Climate Change.[55−59] All emissions are adapted for use in the GEOS-Chem model using the Harvard-NASA Emissions Component (HEMCO) module,[60] and each emission scenario is labeled in accordance with the estimated radiative forcing values for the year 2100. The emission scenarios are run in both base and AmOx configurations to determine the impact
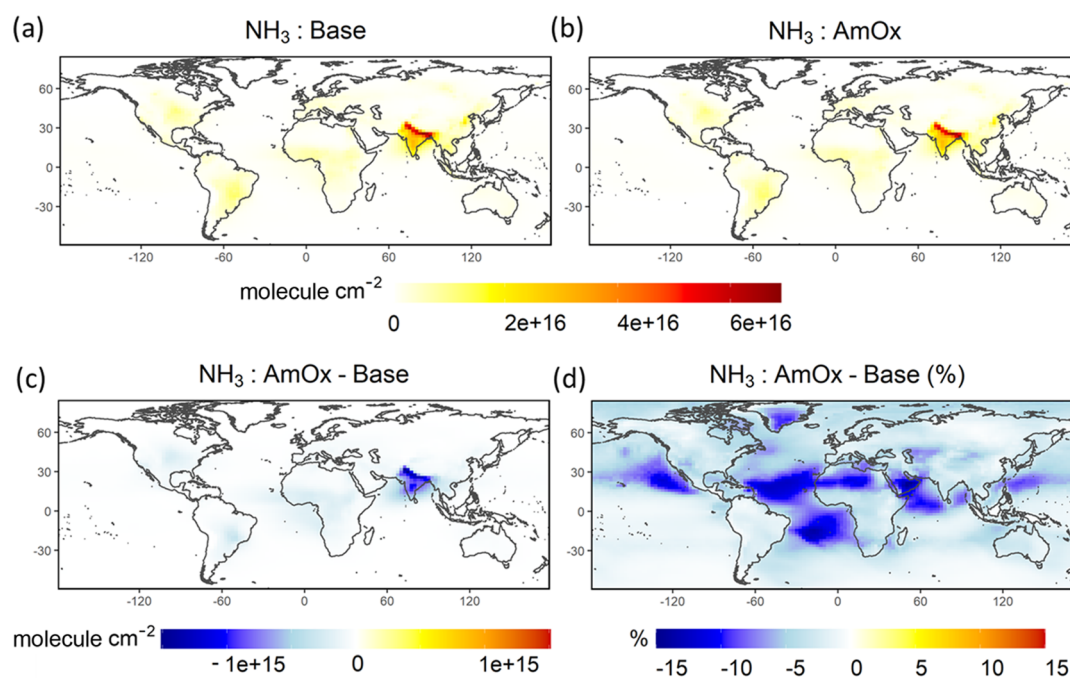
Figure 1. Annual average ammonia column concentrations for the (a) base and (b) AmOx simulations. (c) Absolute difference (in molecule cm^{-2}) between the two simulations. (d) Relative difference (%) between the two simulations. Simulation is for the year 2016. Color bars are saturated at the respective values.

of the ammonia oxidation process under future chemical regimes.

3. RESULTS AND DISCUSSION

3.1. Global Comparison. Figure 1 compares the annual mean column concentrations of ammonia (in molecule cm^{-2}) between the base and AmOx simulations. Ammonia concentrations vary substantially across different regions, with hot spots over India, China, central Africa, and parts of North and South America (Figure 1a,b). These differences reflect the spatial heterogeneity in emissions, driven largely by regions practicing intensive agriculture (Figure S1 illustrates global NH_3 emissions). The inclusion of the AmOx pathway decreases ammonia concentrations globally, with the largest impact in absolute terms over northern India, a region characterized by dense agricultural activity. Section 3.2 provides a more detailed description of the impact of ammonia oxidation over the Indian subcontinent. In relative terms, the most significant reductions in NH_3 are seen over remote outflow regions in aged air masses. Differences in ammonia column burdens can exceed 10% over such regions.

Figure 2a illustrates that ammonia oxidation reduces the annual mean global ammonia burden by approximately 3% (2.2−4.4% across different seasons). Under the MaxNO$_x$ scenario, ammonia burdens are further reduced, approaching up to a monthly averaged reduction of 5% when compared to the base simulation. Global ammonia burdens display a strong bimodal pattern, with local peaks in the March−May and September−November seasons, resulting from the aggregation of different regional sources including agricultural fertilization and crop residue burning.[61] The lifetime of NH_3 against oxidation by OH varies with ambient OH concentrations and is thus lowest in June (Figure 2b) when it is summer in the northern hemisphere. This reflects the disproportionate contribution of NH_3 from the northern hemisphere, which

accounts for between 63 and 82% of the global monthly ammonia burden. However, even at its lowest, the lifetime of NH_3 loss against oxidation is greater than 30 days, significantly longer than the atmospheric lifetime of NH_3 against other processes (such as uptake to particles and dry and wet deposition), which is between 12 and 48 h on average. This underscores the relatively minor role of this pathway in determining the fate of NH_3 at the global scale. Figure 2d−f shows the monthly production of N_2O, NO, and N_2 resulting from the oxidative loss of NH_3 (Figure 2c). The MaxNO$_x$ simulation produces minimal amounts of N_2O, and the MaxN$_2$O simulation produces similarly low levels of NO. The wide range in production estimates illustrates the large uncertainties in the branching ratios and kinetics that govern the preferential production of NO$_x$ or N_2O. The seasonal nature of ammonia emissions,[61] and of ambient OH, results in a strong seasonal signal in the simulated effects of the oxidation mechanism. However, the direction of the response remains consistent across seasons. As a result, we focus our analysis on an annual comparison. The annual production of N_2O is estimated at 0.61 Tg N year^{-1}, with an upper bound of 1.15 Tg N year^{-1} from the MaxN$_2$O simulation. The N_2O production estimates lie within the 0.4−1.2 Tg N annual N_2O production range from previous evaluations of this mechanism.[1,14,20,21] N_2O production from the AmOx and MaxN$_2$O simulations is equivalent to approximately 8 and 16% of the total annual anthropogenic N_2O source, respectively, and would account for a significant fraction of the estimated 17 Tg year^{-1} global N_2O production.[24−27] In terms of radiative forcing, the production of N_2O from the MaxN$_2$O simulation can be viewed as roughly equivalent to the annual addition of 0.54 Pg of CO_2, which is greater than the yearly CO_2 emissions of countries such as Brazil (around 0.47 Pg) and Mexico (around 0.44 Pg).[62] The reaction of NO_2 with NH_2 has also been invoked to explain the mass-independent oxygen isotope fractionation of tropospheric N_2O.[63] An accurate interpreta-
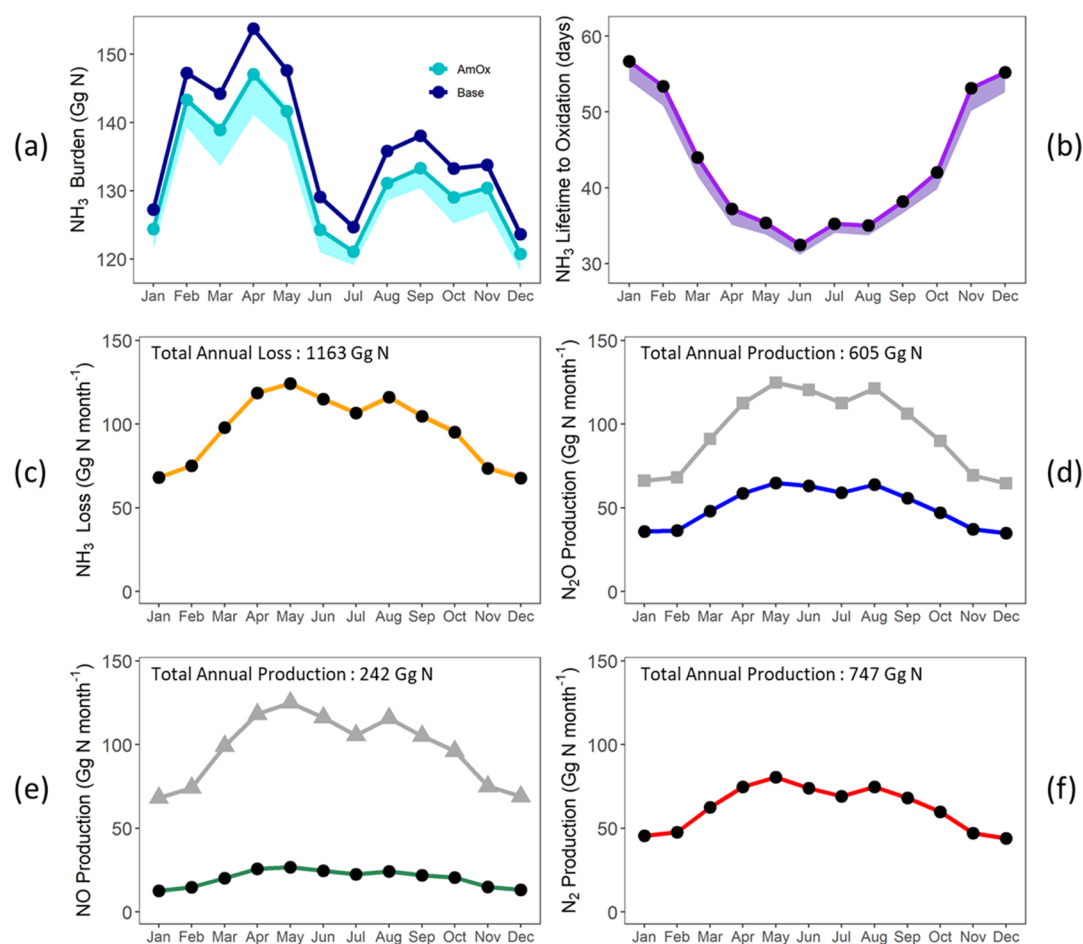
Figure 2. (a) Comparison of the total NH_3 burdens (Gg N) between the base simulation (dark blue) and the AmOx simulation (light blue). (b) Lifetime of atmospheric ammonia against its oxidation with OH. (c) Global monthly loss rate of NH_3 due to its oxidation and the associated production rates of (d) N_2O, (e) NO, and (f) N_2. All results are from a 2016 simulation. Panel (d) includes N_2O production from the $MaxN_2O$ simulation (gray squares), and panel (e) includes NO production from the $MaxNO_x$ simulation (gray triangles). The shaded regions in panels (a)−(c) illustrate the spread in upper- and lower-bound estimates from the two sensitivity simulations.

tion of the N_2O budget using isotopomers might thus require the inclusion of this source.

The annual NO production totals 0.24 Tg N year^{-1}, less than 1% of the total global NO_x source estimated by other studies[28] and around 4% of the 6.3 Tg N year^{-1} source from lightning, which is a similarly diffuse source of oxidized nitrogen in the free troposphere. However, the annual NO production from the $MaxNO_x$ simulation is almost 4 times greater at 1.17 Tg N year^{-1}, although smaller than the upper-bound NO production estimate of 1.6 Tg N year^{-1} by Lee et al.[19] While ammonia oxidation does not result in meaningful NO_x production at the global scale, our simulations indicate that it could influence atmospheric chemistry in remote NO_x-limited regions by serving as a small but relatively important source of NO.

Figure 3 shows how gas-phase concentrations at the surface are impacted by the ammonia oxidation process. Relative differences in ammonia concentrations are most significant over remote ocean environments where they have limited implications for human health but could potentially impact other important microphysical processes like cloud formation.[64] Meaningful differences in NH_3 concentrations (5−10%) also manifest over the African Sahel and the Arabian Peninsula where they could influence regional air quality. There is an increase in surface NO_x concentrations over the

Indian subcontinent and a marked decrease in surface O_3 and OH levels. In this region, the oxidation of ammonia also provides a source of NO_x in the lower FT (Figure S3). Following export to more NO_x-limited environments, this excess NO_x eventually contributes to an increased global production of O_3 in the FT, resulting in a marginal increase in surface-level O_3 concentrations over much of the globe (Figures 3b and S4). OH displays a similar response, with lower concentrations over continental regions but higher concentrations over the oceans (Figure 3c), responding to complex and nonlinear effects from the increase in ambient NO_x concentrations over these regions that promote more efficient HO_x cycling. The increase in oxidative capacity over remote ocean environments could influence chemistry and microphysics in these regions, such as the formation of cloud condensation nuclei and ice-nucleating particles. Given the large ammonia source over the Indian subcontinent, changes in atmospheric composition are most pronounced in this region. We discuss these in detail in Section 3.2.

In addition to the impact on key gas-phase species, NH_3 oxidation influences SNA aerosol concentrations. Global inorganic aerosol burdens decrease with the inclusion of the ammonia oxidation pathway, with ammonium burdens lower by roughly 6 Gg globally (2%) and nitrate burdens lower by 12 Gg (4%). The impacts on surface concentrations for these
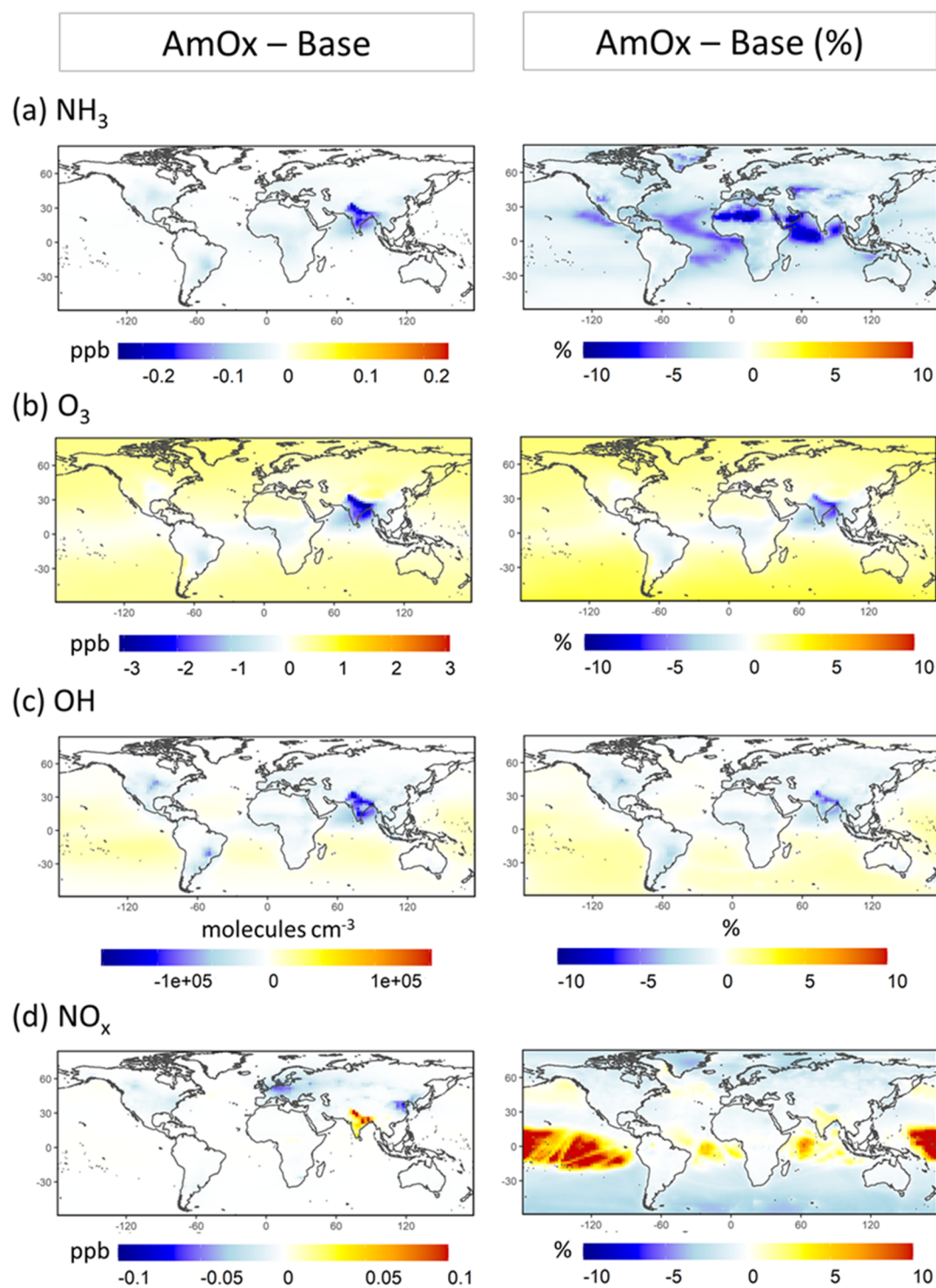
Figure 3. Comparison of annual average gas-phase concentrations at the surface between the base and AmOx model simulations for (a) NH_3, (b) O_3, (c) OH, and (d) NO_x (NO + NO_2). Figure S2 provides a similar comparison at the model pressure level of 500 hPa.

species are shown in Figure 4. Nitrate formation is extremely sensitive to ambient ammonia availability, and the spatial patterns of the nitrate reductions in Figure 4 track the regional decreases in ammonia. Relative differences between 5 and 10% in NO_3^- concentrations also manifest over Africa, Central America, and parts of South America. In pristine regions, such as the forests of South America, these reductions (on the order of 5%) could be important to regional aerosol chemistry by impacting aerosol acidity, inorganic aerosol partitioning, and

organic nitrate formation. The increase in ammonium nitrate concentrations over remote ocean environments is driven by an increase in NO_x over these regions (Figure 3). Sulfate burdens are relatively unaffected at the global scale. When viewed in aggregate, the impact of the ammonia oxidation pathway is to reduce inorganic surface $PM_{2.5}$ concentrations over most continental regions, resulting in a marginal improvement in simulated air quality.
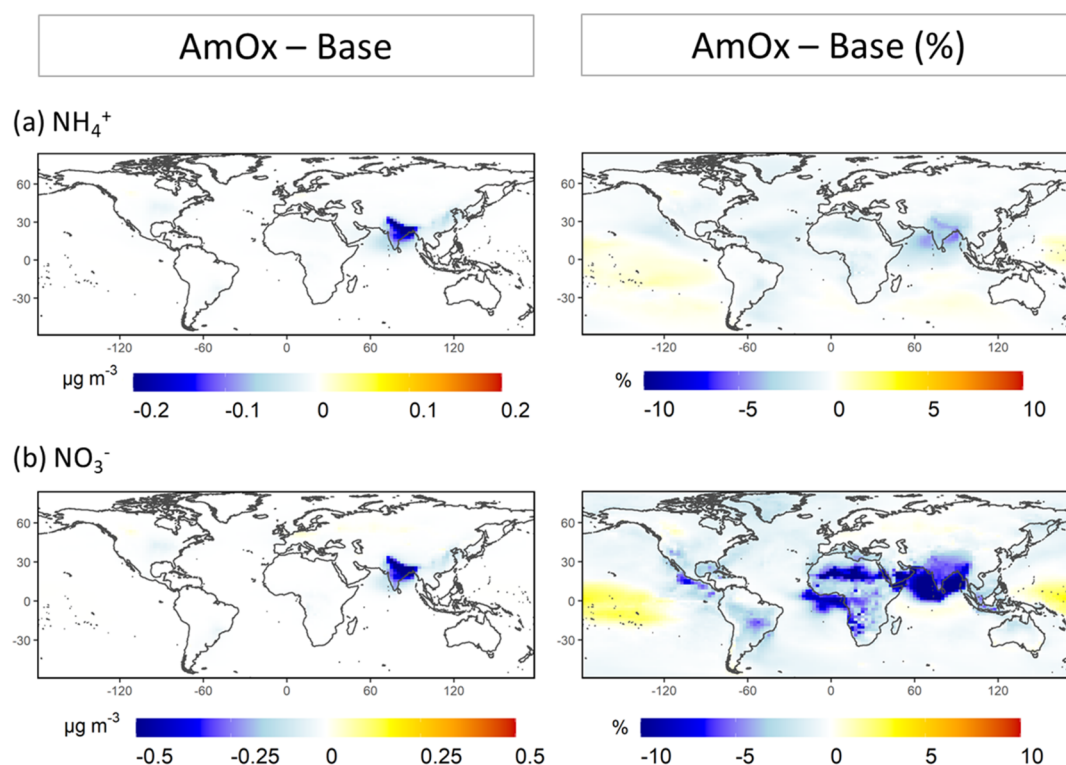
Figure 4. Comparison of the annual average aerosol concentrations at the surface between the base and AmOx model simulations for (a) ammonium and (b) nitrate aerosol.

As a function of altitude, the inclusion of the oxidation process decreases NH_3 concentrations throughout the troposphere, with reductions between 2 and 10% (Figure S4). A recent study suggests that CTMs overestimate ammonia concentrations in the FT and may be missing an important NH_3 loss mechanism;[65] ammonia oxidation by OH could contribute to this missing loss. Global profiles for NO, HNO_3, OH, O_3, and SO_4^{2-} in the lower troposphere are largely unchanged (less than 5%), with the impact of the ammonia oxidation pathway most apparent on the ammonium and nitrate profiles.

3.2. Regional Comparison over the Indian Subcontinent. While ammonia oxidation has meaningful implications for global N_2O production, its impact on other key atmospheric species is relatively minor at the global scale. However, as indicated in Section 3.1, it can play a more substantial role at the regional level, particularly over the Indian subcontinent, which is the dominant contributor to global ammonia emissions. The absolute impact from the AmOx mechanism on NH_3 concentrations is thus greatest over India, where it also contributes the most NO_x in absolute terms.

Figure 5 illustrates the impact of the oxidation pathway on surface concentrations of NH_3, NO_x, OH, O_3, NH_4^+, and NO_3^- over the Indian subcontinent. Figure S5 provides the same comparison as a relative difference. The effect on these species is significant, with O_3 and particulate NO_3^- decreasing by around 3 ppb and 1 $\mu g\ m^{-3}$, respectively, over parts of northern India. Surface OH concentrations drop by up to 7% over some areas of northern India, largely due to nonlinear interactions with the NO_x perturbations. In addition to its impact on surface concentrations, ammonia oxidation also influences the vertical distributions of OH and O_3 over the

Indian subcontinent (Figure S6). The inclusion of the ammonia oxidation pathway also impacts the relative abundance of SNA species over this region, decreasing the NH_4^+/SO_4^{2-} ratio and increasing the NH_4^+/NO_3^- ratio. Changes in bulk SNA ionic ratios have important implications for particle acidity and pH, particularly in the free troposphere where our simulations estimate meaningful changes in particulate pH (Figure S7). The impact of the oxidation mechanism on aerosol pH is consistent in sign with the recent work that has suggested that CTMs underestimate aerosol acidity in remote environments.[65] These changes could also influence a number of other important aerosol interactions that influence particle growth and heterogeneous chemistry.[4,66,67]

3.3. Evaluating the Importance of NH_3 Oxidation under Future Emissions Scenarios. Global ammonia emissions are anticipated to continue increasing over much of the 21st century in response to increasing agricultural demand. This is juxtaposed against a decreasing trend in global NO_x emissions that is similarly predicted to continue with increased regulatory pressure worldwide. Given these opposing trends, the atmospheric composition of reactive nitrogen under future scenarios can be expected to deviate substantially from that of the present, with a progressive shift in total N emissions toward NH_3. This shift in composition could magnify the importance of ammonia oxidation as a source of global N_2O and as a regional source of NO_x given the reduced emissions from other sources. To estimate the importance of this mechanism under future scenarios, we utilize a series of simulations conducted using four different emission scenarios, set in the year 2100, using the representative concentration pathway (RCP) framework outlined in Section 2. NH_3 and NO_x emissions vary across the scenarios but in general exhibit similar trends of increasing NH_3 emissions and decreasing
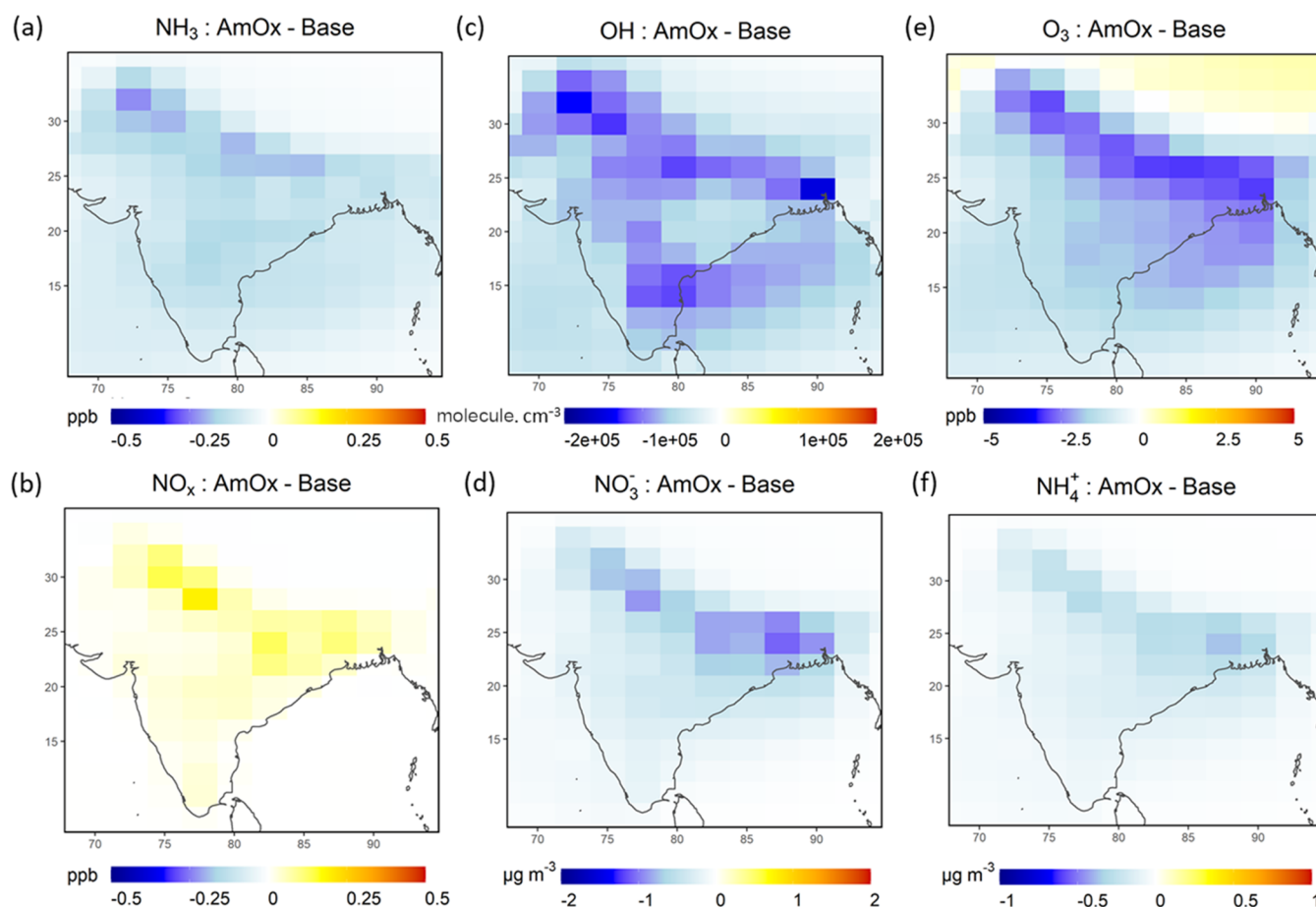
Figure 5. Comparison of the annual average aerosol concentrations at the surface between the base and AmOx model simulations for (a) NH_3, (b) NO_x, (c) OH, (d) NO_3^-, (e) O_3, and (f) NH_4^+ over the Indian subcontinent.
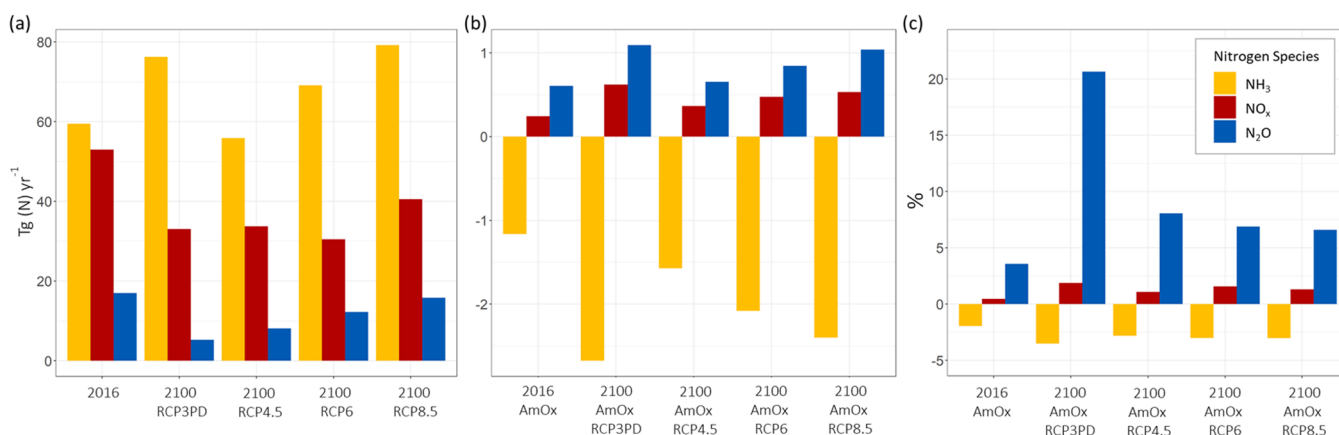

Figure 6. (a) Global annual NH_3, NO_x (NO + NO_2), and N_2O emissions in Tg N across the RCP scenarios compared to the baseline emissions used to drive the 2016 simulation. (b) Total annual change in the source of key species across the RCP scenarios in Tg N compared to that of the AmOx simulation for 2016. (c) Change in the annual source of key species across the scenarios relative to their total sources. The representative concentration pathways (RCPs) are labeled with their associated radiative forcing (e.g., 8.5 W m^{-2}); RCP 3PD refers to a "peak-and-decline" scenario corresponding to a radiative forcing of 2.6 W m^{-2}. N_2O is not directly emitted into the model but is provided here for context. 2016 N_2O emissions are based on the estimate from Tian et al.,[27] and 2100 global N_2O global emissions are from the IIASA RCP database.[68]

NO_x emissions (Figure 6a). Simulations conducted both with and without the AmOx mechanism for each RCP scenario indicate that ammonia oxidation could become a substantial global source of N_2O in the future, with annual estimates ranging from 0.65 to 1.10 Tg N (Figure 6b), potentially accounting for a large fraction of global N_2O emissions (7–

21%) in the year 2100.[68,69] Similarly, the increased ammonia burden results in a larger (though still relatively small) NO_x source, equivalent to between 1.1 and 1.9% of estimated global NO_x emissions in 2100 (Figure 6c). In general, the impact of the ammonia oxidation process under the future scenarios is to deplete O_3 and OH across continental regions while increasing

the concentrations of these oxidants in the remote southern hemisphere. The increase in NO_x concentrations from NH_3 oxidation over the Indian subcontinent has particularly significant consequences for regional oxidative chemistry, decreasing surface-level ozone by up to 6 ppb in the RCP 3PD scenario and reducing nitrate and ammonium aerosol concentrations by between 5 and 20% in many regions across all scenarios. These results suggest that the ammonia oxidation process will take on an increased importance in the future atmosphere, further reinforcing the need to constrain the kinetics of this process.

4. CONCLUSIONS

The atmospheric oxidation of ammonia is typically not included within the current global chemical transport models. In this study, we incorporate an explicit mechanism to simulate ammonia oxidation initiated by the OH radical. Using a global model simulation for 2016, we find that the annual oxidation loss of NH_3 is considerably smaller than other removal pathways, resulting in an average annual reduction of approximately 3% in the global ammonia burden. These changes are well within the observational uncertainties driving global ammonia estimates, indicating that the addition of this mechanism is unlikely to meaningfully improve model NH_3 simulations. While other drivers of uncertainty, such as the treatment of NH_3 emissions, partitioning, and deposition, are more important avenues for future research to constrain the fate of atmospheric NH_3, the oxidation process could be a significant removal mechanism in remote environments.

Despite its relatively small influence on global NH_3 concentrations, the annual N_2O production from NH_3 oxidation is estimated to be 8% (with an upper bound of 16%) of the total anthropogenic N_2O emissions from other sources, with significant implications for radiative forcing estimates. Our analysis also suggests that ammonia oxidation could account for up to 21% of the total N_2O source (potentially even more using $MaxN_2O$ conditions) under future climatic scenarios. These results stress the importance of the agriculture sector as an indirect source of an important greenhouse gas. Our analysis suggests that global climate models and earth system models would benefit from the incorporation of an explicit ammonia oxidation mechanism when modeling N_2O, with the caveat that additional laboratory studies need to be conducted to better constrain its production from this pathway.

While ammonia oxidation is currently not an important global source of NO, this study demonstrates that the pathway could impact key atmospheric species at regional scales, with a particularly clear influence over the Indian subcontinent. Surface concentrations of OH and O_3 see regional reductions of over 5%, with potential consequences for oxidative chemistry and for determining the policy-relevant background concentrations for various key species. Surface $PM_{2.5}$ concentrations are similarly impacted, with decreases in ammonium and nitrate aerosol loadings of up to 4 and 9%, respectively. Perturbing the available gas-phase ammonia over polluted regions also impacts the relative ratios of the SNA ions, influencing aerosol acidity and particle pH. Despite the importance of these interactions, sensitivity simulations demonstrate large uncertainties in the NO production estimates, supporting the need for more research. To more comprehensively assess the magnitude of the atmospheric response to ammonia oxidation over India and other regions of interest, additional work is necessary to constrain the underlying NH_3 simulation over these regions by validating process-level drivers of uncertainty from model emissions, transport, physical loss, and other chemical and thermodynamic interactions.

With ammonia emissions expected to increase in the coming decades, our analysis using a series of RCP simulations suggests that the atmospheric oxidation of ammonia will become an increasingly important source of N_2O and remote NO_x under future climate scenarios. Given the growing atmospheric influence of this process, additional research is needed to constrain this pathway (and the associated reaction parameters) to more accurately simulate the impact of future ammonia emissions on global atmospheric chemistry and climate.

■ ASSOCIATED CONTENT

Ⓢ Supporting Information

The Supporting Information is available free of charge at https://pubs.acs.org/doi/10.1021/acsearthspace-chem.1c00021.

> Global annual average ammonia emissions (Figure S1); comparison of annual average gas-phase concentrations at the model pressure level of 500 hPa between the base and AmOx model simulations for NH_3, O_3, OH, and NO_x (Figure S2); vertical profiles of the global annual mean loss of NH_3 and production of NO via the ammonia oxidation pathway for the AmOx simulation in 2016 (Figure S3); comparison of annual average vertical profiles for key atmospheric species over the entire globe and over the Indian subcontinent (Figure S4); a relative comparison of annual average aerosol concentrations at the surface between the base and AmOx model simulations for key atmospheric species over the Indian subcontinent (Figure S5); vertical profiles for key atmospheric species over the Indian subcontinental region for the base and AmOx simulations (Figure S6); and changes in the simulated particle pH at the 500 hPa pressure level between the base and AmOx simulations (Figure S7) (PDF)

■ AUTHOR INFORMATION

Corresponding Authors

Sidhant J. Pai − *Department of Civil and Environmental Engineering, Massachusetts Institute of Technology, Cambridge, Massachusetts 02139, United States;* ⓞ orcid.org/0000-0003-3977-4495; Email: sidhantp@mit.edu

Jennifer G. Murphy − *Department of Chemistry, University of Toronto, Toronto, Ontario M5S 3H6, Canada;* ⓞ orcid.org/0000-0001-8865-5463; Email: jen.murphy@utoronto.ca

Author

Colette L. Heald − *Department of Civil and Environmental Engineering, Massachusetts Institute of Technology, Cambridge, Massachusetts 02139, United States;* ⓞ orcid.org/0000-0003-2894-5738

Complete contact information is available at:
https://pubs.acs.org/10.1021/acsearthspacechem.1c00021

Author Contributions

J.G.M. conceived the idea and developed the chemical mechanism. C.L.H. and S.J.P. designed the modeling study. S.J.P. performed the simulations and analysis. S.J.P., C.L.H., and J.G.M. wrote the manuscript.

Notes

The authors declare no competing financial interest.

■ REFERENCES

(1) Dentener, F. J.; Crutzen, P. J. A Three-Dimensional Model of the Global Ammonia Cycle. *J. Atmos. Chem.* **1994**, *19*, 331−333.

(2) Camargo, J. A.; Alonso, Á. Ecological and Toxicological Effects of Inorganic Nitrogen Pollution in Aquatic Ecosystems: A Global Assessment. *Environ. Int.* **2006**, *32*, 831−849.

(3) Krupa, S. V. Effects of Atmospheric Ammonia (NH3) on Terrestrial Vegetation: A Review. *Environ. Pollut.* **2003**, *124*, 179−221.

(4) Pozzer, A.; Tsimpidi, A. P.; Karydis, V. A.; de Meij, A.; Lelieveld, J. Impact of Agricultural Emission Reductions on Fine-Particulate Matter and Public Health. *Atmos. Chem. Phys.* **2017**, *17*, 12813−12826.

(5) Bellouin, N.; Rae, J.; Jones, A.; Johnson, C.; Haywood, J.; Boucher, O. Aerosol Forcing in the Climate Model Intercomparison Project (CMIP5) Simulations by HadGEM2-ES and the Role of Ammonium Nitrate. *J. Geophys. Res.: Atmos.* **2011**, *116*, No. D20206.

(6) Cohen, A. J.; Brauer, M.; Burnett, R.; Anderson, H. R.; Frostad, J.; Estep, K.; Balakrishnan, K.; Brunekreef, B.; Dandona, L.; Dandona, R.; Feigin, V.; Freedman, G.; Hubbell, B.; Jobling, A.; Kan, H.; Knibbs, L.; Liu, Y.; Martin, R.; Morawska, L.; Pope, C. A.; Shin, H.; Straif, K.; Shaddick, G.; Thomas, M.; van Dingenen, R.; van Donkelaar, A.; Vos, T.; Murray, C. J. L.; Forouzanfar, M. H. Estimates and 25-Year Trends of the Global Burden of Disease Attributable to Ambient Air Pollution: An Analysis of Data from the Global Burden of Diseases Study 2015. *Lancet* **2017**, *389*, 1907−1918.

(7) Pope, C. A.; Dockery, D. W. Health Effects of Fine Particulate Air Pollution: Lines That Connect. *J. Air Waste Manage. Assoc.* **2006**, *56*, 709−742.

(8) Bouwman, A. F.; Lee, D. S.; Asman, W. A. H.; Dentener, F. J.; Van Der Hoek, K. W.; Olivier, J. G. J. A Global High-Resolution Emission Inventory for Ammonia. *Global Biogeochem. Cycles* **1997**, *11*, 561−587.

(9) Erisman, J. W.; Sutton, M. A.; Galloway, J.; Klimont, Z.; Winiwarter, W. How a Century of Ammonia Synthesis Changed the World. *Nat. Geosci.* **2008**, *1*, 636−639.

(10) Xu, R. T.; Pan, S. F.; Chen, J.; Chen, G. S.; Yang, J.; Dangal, S. R. S.; Shepard, J. P.; Tian, H. Q. Half-Century Ammonia Emissions From Agricultural Systems in Southern Asia: Magnitude, Spatiotemporal Patterns, and Implications for Human Health. *GeoHealth* **2018**, *2*, 40−53.

(11) Krotkov, N. A.; McLinden, C. A.; Li, C.; Lamsal, L. N.; Celarier, E. A.; Marchenko, S. V.; Swartz, W. H.; Bucsela, E. J.; Joiner, J.; Duncan, B. N.; Boersma, K. F.; Veefkind, J. P.; Levelt, P. F.; Fioletov, V. E.; Dickerson, R. R.; He, H.; Lu, Z.; Streets, D. G. Aura OMI Observations of Regional SO_2 and NO_2 Pollution Changes from 2005 to 2015. *Atmos. Chem. Phys.* **2016**, *16*, 4605−4629.

(12) Pinder, R. W.; Appel, K. W.; Dennis, R. L. Trends in Atmospheric Reactive Nitrogen for the Eastern United States. *Environ. Pollut.* **2011**, *159*, 3138−3141.

(13) Logan, J. A. Nitrogen Oxides in the Troposphere: Global and Regional Budgets. *J. Geophys. Res.: Oceans* **1983**, *88*, 10785−10807.

(14) Kohlmann, J.-P.; Poppe, D. The Tropospheric Gas-Phase Degradation of NH3 and Its Impact on the Formation of N2O and NOx. *J. Atmos. Chem.* **1999**, *32*, 397−415.

(15) Sun, F.; DeSain, J. D.; Scott, G.; Hung, P. Y.; Thompson, R. I.; Glass, G. P.; Curl, R. F. Reactions of NH2 with NO2 and of OH with NH2O. *J. Phys. Chem. A* **2001**, *105*, 6121−6128.

(16) Bulatov, V. P.; Buloyan, A. A.; Cheskis, S. G.; Kozliner, M. Z.; Sarkisov, O. M.; Trostin, A. I. On the Reaction of the NH2 Radical with Ozone. *Chem. Phys. Lett.* **1980**, *74*, 288−292.

(17) Dammers, E.; McLinden, C. A.; Griffin, D.; Shephard, M. W.; Van Der Graaf, S.; Lutsch, E.; Schaap, M.; Gainairu-Matz, Y.; Fioletov, V.; Van Damme, M.; Whitburn, S.; Clarisse, L.; Cady-Pereira, K.; Clerbaux, C.; Coheur, P. F.; Erisman, J. W. NH_3 Emissions from Large Point Sources Derived from CrIS and IASI Satellite Observations. *Atmos. Chem. Phys.* **2019**, *19*, 12261−12293.

(18) Van Damme, M.; Clarisse, L.; Whitburn, S.; Hadji-Lazaro, J.; Hurtmans, D.; Clerbaux, C.; Coheur, P.-F. Industrial and Agricultural Ammonia Point Sources Exposed. *Nature* **2018**, *564*, 99−103.

(19) Lee, D. S.; Köhler, I.; Grobler, E.; Rohrer, F.; Sausen, R.; Gallardo-Klenner, L.; Olivier, J. G. J.; Dentener, F. J.; Bouwman, A. F. Estimations of Global No, Emissions and Their Uncertainties. *Atmos. Environ.* **1997**, *31*, 1735−1749.

(20) Khan, M. A. H.; Lowe, D.; Derwent, R. G.; Foulds, A.; Chhantyal-Pun, R.; McFiggans, G.; Orr-Ewing, A. J.; Percival, C. J.; Shallcross, D. E. Global and Regional Model Simulations of Atmospheric Ammonia. *Atmos. Res.* **2020**, *234*, No. 104702.

(21) Hauglustaine, D. A.; Balkanski, Y.; Schulz, M. A Global Model Simulation of Present and Future Nitrate Aerosols and Their Direct Radiative Forcing of Climate. *Atmos. Chem. Phys.* **2014**, *14*, 11031−11063.

(22) Adams, P. J.; Seinfeld, J. H.; Koch, D. M. Global Concentrations of Tropospheric Sulfate, Nitrate, and Ammonium Aerosol Simulated in a General Circulation Model. *J. Geophys. Res.: Atmos.* **1999**, *104*, 13791−13823.

(23) Xu, L.; Penner, J. E. Global Simulations of Nitrate and Ammonium Aerosols and Their Radiative Effects. *Atmos. Chem. Phys.* **2012**, *12*, 9479−9504.

(24) Ciais, P.; Sabine, C.; Bala, G.; Bopp, L.; Brovkin, V.; Canadell, J.; Chhabra, A.; DeFries, R.; Galloway, J.; Heimann, M.; Jones, C.; Le Quere, C.; Myneni, R. B.; Piao, S.; Thornton, P. In *Carbon and Other Biogeochemical Cycles*, IPCC, 2013: Climate Change 2013: The Physical Science Basis. Contribution of Working Group I to the Fifth Assessment Report of the Intergovernmental Panel on Climate Change; Cambridge University Press: Cambridge, 2013.

(25) Myhre, G.; Shindell, D.; Bréon, F.-M.; Collins, W.; Fuglestvedt, J.; Huang, J.; Koch, D.; Lamarque, J.-F.; Lee, D.; Mendoza, B.; Nakajima, T.; Robock, A.; Stephens, G.; Zhang, H.; Aamaas, B.; Boucher, O.; Dalsøren, S. B.; Daniel, J. S.; Forster, P.; Granier, C.; Haigh, J.; Hodnebrog, Ø.; Kaplan, J. O.; Marston, G.; Nielsen, C. J.; O'Neill, B. C.; Peters, G. P.; Pongratz, J.; Ramaswamy, V.; Roth, R.; Rotstayn, L.; Smith, S. J.; Stevenson, D.; Vernier, J.-P.; Wild, O.; Young, P.; Jacob, D.; Ravishankara, A. R.; Shine, K. In *Anthropogenic and Natural Radiative Forcing*, IPCC, 2013: Climate Change 2013: The Physical Science Basis. Contribution of Working Group I to the Fifth Assessment Report of the Intergovernmental Panel on Climate Change; Cambridge University Press: Cambridge, 2013; p 82.

(26) Tian, H.; Yang, J.; Lu, C.; Xu, R.; Canadell, J. G.; Jackson, R. B.; Arneth, A.; Chang, J.; Chen, G.; Ciais, P.; Gerber, S.; Ito, A.; Huang, Y.; Joos, F.; Lienert, S.; Messina, P.; Olin, S.; Pan, S.; Peng, C.; Saikawa, E.; Thompson, R. L.; Vuichard, N.; Winiwarter, W.; Zaehle, S.; Zhang, B.; Zhang, K.; Zhu, Q. The Global N $_2$ O Model Intercomparison Project. *Bull. Am. Meteorol. Soc.* **2018**, *99*, 1231−1251.

(27) Tian, H.; Xu, R.; Canadell, J. G.; Thompson, R. L.; Winiwarter, W.; Suntharalingam, P.; Davidson, E. A.; Ciais, P.; Jackson, R. B.; Janssens-Maenhout, G.; Prather, M. J.; Regnier, P.; Pan, N.; Pan, S.; Peters, G. P.; Shi, H.; Tubiello, F. N.; Zaehle, S.; Zhou, F.; Arneth, A.; Battaglia, G.; Berthet, S.; Bopp, L.; Bouwman, A. F.; Buitenhuis, E. T.; Chang, J.; Chipperfield, M. P.; Dangal, S. R. S.; Dlugokencky, E.; Elkins, J. W.; Eyre, B. D.; Fu, B.; Hall, B.; Ito, A.; Joos, F.; Krummel, P. B.; Landolfi, A.; Laruelle, G. G.; Lauerwald, R.; Li, W.; Lienert, S.; Maavara, T.; MacLeod, M.; Millet, D. B.; Olin, S.; Patra, P. K.; Prinn,

R. G.; Raymond, P. A.; Ruiz, D. J.; van der Werf, G. R.; Vuichard, N.; Wang, J.; Weiss, R. F.; Wells, K. C.; Wilson, C.; Yang, J.; Yao, Y. A Comprehensive Quantification of Global Nitrous Oxide Sources and Sinks. *Nature* **2020**, *586*, 248−256.

(28) Geddes, J. A.; Martin, R. V. Global Deposition of Total Reactive Nitrogen Oxides from 1996 to 2014 Constrained with Satellite Observations of NO_2 Columns. *Atmos. Chem. Phys.* **2017**, *17*, 10071−10091.

(29) Jacob, D. J.; Logan, J. A.; Gardner, G. M.; Yevich, R. M.; Spivakovsky, C. M.; Wofsy, S. C.; Sillman, S.; Prather, M. J. Factors Regulating Ozone over the United States and Its Export to the Global Atmosphere. *J. Geophys. Res.: Atmos.* **1993**, *98*, 14817−14826.

(30) Hudman, R. C.; Jacob, D. J.; Turquety, S.; Leibensperger, E. M.; Murray, L. T.; Wu, S.; Gilliland, A. B.; Avery, M.; Bertram, T. H.; Brune, W.; Cohen, R. C.; Dibb, J. E.; Flocke, F. M.; Fried, A.; Holloway, J.; Neuman, J. A.; Orville, R.; Perring, A.; Ren, X.; Sachse, G. W.; Singh, H. B.; Swanson, A.; Wooldridge, P. J. Surface and Lightning Sources of Nitrogen Oxides over the United States: Magnitudes, Chemical Evolution, and Outflow. *J. Geophys. Res.: Atmos.* **2007**, *112*, No. D12S05.

(31) GEOS-Chem. Geoschem/Geos-Chem: GEOS-Chem 12.1.1. *Zenodo* **2018**, DOI: 10.5281/zenodo.2249246.

(32) Philip, S.; Martin, R. V.; Keller, C. A. Sensitivity of Chemistry-Transport Model Simulations to the Duration of Chemical and Transport Operators: A Case Study with GEOS-Chem V10-01. *Geosci. Model Dev.* **2016**, *9*, 1683−1695.

(33) Mao, J.; Paulot, F.; Jacob, D. J.; Cohen, R. C.; Crounse, J. D.; Wennberg, P. O.; Keller, C. A.; Hudman, R. C.; Barkley, M. P.; Horowitz, L. W. Ozone and Organic Nitrates over the Eastern United States: Sensitivity to Isoprene Chemistry. *J. Geophys. Res.: Atmos.* **2013**, *118*, 11256−11268.

(34) Miller, C. C.; Jacob, D. J.; Marais, E. A.; Yu, K.; Travis, K. R.; Kim, P. S.; Fisher, J. A.; Zhu, L.; Wolfe, G. M.; Hanisco, T. F.; Keutsch, F. N.; Kaiser, J.; Min, K.-E.; Brown, S. S.; Washenfelder, R. A.; González Abad, G.; Chance, K. Glyoxal Yield from Isoprene Oxidation and Relation to Formaldehyde: Chemical Mechanism, Constraints from SENEX Aircraft Observations, and Interpretation of OMI Satellite Data. *Atmos. Chem. Phys.* **2017**, *17*, 8725−8738.

(35) Travis, K. R.; Jacob, D. J.; Fisher, J. A.; Kim, P. S.; Marais, E. A.; Zhu, L.; Yu, K.; Miller, C. C.; Yantosca, R. M.; Sulprizio, M. P.; Thompson, A. M.; Wennberg, P. O.; Crounse, J. D.; St Clair, J. M.; Cohen, R. C.; Laughner, J. L.; Dibb, J. E.; Hall, S. R.; Ullmann, K.; Wolfe, G. M.; Pollack, I. B.; Peischl, J.; Neuman, J. A.; Zhou, X. Why Do Models Overestimate Surface Ozone in the Southeast United States? *Atmos. Chem. Phys.* **2016**, *16*, 13561−13577.

(36) Sherwen, T.; Schmidt, J. A.; Evans, M. J.; Carpenter, L. J.; Großmann, K.; Eastham, S. D.; Jacob, D. J.; Dix, B.; Koenig, T. K.; Sinreich, R.; Ortega, I.; Volkamer, R.; Saiz-Lopez, A.; Prados-Roman, C.; Mahajan, A. S.; Ordóñez, C. Global Impacts of Tropospheric Halogens (Cl, Br, I) on Oxidants and Composition in GEOS-Chem. *Atmos. Chem. Phys.* **2016**, *16*, 12239−12271.

(37) Fountoukis, C.; Nenes, A. ISORROPIA II: A Computationally Efficient Thermodynamic Equilibrium Model for K+−Ca2+−Mg2+−NH4+−Na+−SO24−−NO−3 −Cl−−H2O Aerosols. *Atmos. Chem. Phys.* **2007**, *7*, 4639−4659.

(38) IUPAC. IUPAC Task Group on Atmospheric Chemical Kinetic Data Evaluation—Data Sheet NOx22, 2001, pp 1−3.

(39) Burkholder, J. B.; Sander, S. P.; Abbatt, J.; Barker, J. R.; Huie, R. E.; Kolb, C. E.; Kurylo, M. J.; Orkin, V. L.; Wilmouth, D. M.; Wine, P. H. Chemical Kinetics and Photochemical Data for Use in Atmospheric Studies, Evaluation No. 18, 2015.

(40) Glarborg, P.; Hashemi, H.; Cheskis, S.; Jasper, A. W. On the Rate Constant for NH_2 +HO_2 and Third-Body Collision Efficiencies for NH_2 +H(+M) and NH_2 +NH_2 (+M). *J. Phys. Chem. A* **2021**, *125*, 1505−1516.

(41) Atkinson, R.; Baulch, D. L.; Cox, R. A.; Crowley, J. N.; Hampson, R. F.; Hynes, R. G.; Jenkin, M. E.; Rossi, M. J.; Troe, J. Evaluated Kinetic and Photochemical Data for Atmospheric

Chemistry: Volume I - Gas Phase Reactions of O_x, HO_x, NO_x and SO_x Species. *Atmos. Chem. Phys.* **2004**, *4*, 1461−1738.

(42) Lin, M. C.; He, Y.; Melius, C. F. Theoretical Interpretation of the Kinetics and Mechanisms of the HNO + HNO and HNO + 2NO Reactions with a Unified Model. *Int. J. Chem. Kinet.* **1992**, *24*, 489−516.

(43) Hoesly, R. M.; Smith, S. J.; Feng, L.; Klimont, Z.; Janssens-Maenhout, G.; Pitkanen, T.; Seibert, J. J.; Vu, L.; Andres, R. J.; Bolt, R. M.; Bond, T. C.; Dawidowski, L.; Kholod, N.; Kurokawa, J.; Li, M.; Liu, L.; Lu, Z.; Moura, M. C. P.; O'Rourke, P. R.; Zhang, Q. Historical (1750−2014) Anthropogenic Emissions of Reactive Gases and Aerosols from the Community Emissions Data System (CEDS). *Geosci. Model Dev.* **2018**, *11*, 369−408.

(44) Li, M.; Zhang, Q.; Kurokawa, J.; Woo, J.-H.; He, K.; Lu, Z.; Ohara, T.; Song, Y.; Streets, D. G.; Carmichael, G. R.; Cheng, Y.; Hong, C.; Huo, H.; Jiang, X.; Kang, S.; Liu, F.; Su, H.; Zheng, B. MIX: A Mosaic Asian Anthropogenic Emission Inventory under the International Collaboration Framework of the MICS-Asia and HTAP. *Atmos. Chem. Phys.* **2017**, *17*, 935−963.

(45) Murray, L. T.; Jacob, D. J.; Logan, J. A.; Hudman, R. C.; Koshak, W. J. Optimized Regional and Interannual Variability of Lightning in a Global Chemical Transport Model Constrained by LIS/OTD Satellite Data. *J. Geophys. Res.: Atmos.* **2012**, *117*, No. D20307.

(46) Ott, L. E.; Pickering, K. E.; Stenchikov, G. L.; Allen, D. J.; DeCaria, A. J.; Ridley, B.; Lin, R.-F.; Lang, S.; Tao, W.-K. Production of Lightning NO_x and Its Vertical Distribution Calculated from Three-Dimensional Cloud-Scale Chemical Transport Model Simulations. *J. Geophys. Res.* **2010**, *115*, No. D04301.

(47) Hudman, R. C.; Moore, N. E.; Mebust, A. K.; Martin, R. V.; Russell, A. R.; Valin, L. C.; Cohen, R. C. Steps towards a Mechanistic Model of Global Soil Nitric Oxide Emissions: Implementation and Space Based-Constraints. *Atmos. Chem. Phys.* **2012**, *12*, 7779−7795.

(48) Holmes, C. D.; Prather, M. J.; Vinken, G. C. M. The Climate Impact of Ship NO_x Emissions: An Improved Estimate Accounting for Plume Chemistry. *Atmos. Chem. Phys.* **2014**, *14*, 6801−6812.

(49) Guenther, A. B.; Jiang, X.; Heald, C. L.; Sakulyanontvittaya, T.; Duhl, T.; Emmons, L. K.; Wang, X. The Model of Emissions of Gases and Aerosols from Nature Version 2.1 (MEGAN2.1): An Extended and Updated Framework for Modeling Biogenic Emissions. *Geosci. Model Dev.* **2012**, *5*, 1471−1492.

(50) van der Werf, G. R.; Randerson, J. T.; Giglio, L.; van Leeuwen, T. T.; Chen, Y.; Rogers, B. M.; Mu, M.; van Marle, M. J. E.; Morton, D. C.; Collatz, G. J.; Yokelson, R. J.; Kasibhatla, P. S. Global Fire Emissions Estimates during 1997−2016. *Earth Syst. Sci. Data* **2017**, *9*, 697−720.

(51) Wesely, M. L. Parameterization of Surface Resistances to Gaseous Dry Deposition in Regional-Scale Numerical Models. *Atmos. Environ. (1967)* **1989**, *23*, 1293−1304.

(52) Zhang, L.; Gong, S.; Padro, J.; Barrie, L. A Size-Segregated Particle Dry Deposition Scheme for an Atmospheric Aerosol Module. *Atmos. Environ.* **2001**, *35*, 549−560.

(53) Amos, H. M.; Jacob, D. J.; Holmes, C. D.; Fisher, J. A.; Wang, Q.; Yantosca, R. M.; Corbitt, E. S.; Galarneau, E.; Rutter, A. P.; Gustin, M. S.; Steffen, A.; Schauer, J. J.; Graydon, J. A.; St Louis, V. L.; Talbot, R. W.; Edgerton, E. S.; Zhang, Y.; Sunderland, E. M. Gas-Particle Partitioning of Atmospheric Hg(II) and Its Effect on Global Mercury Deposition. *Atmos. Chem. Phys.* **2012**, *12*, 591−603.

(54) Liu, H.; Jacob, D. J.; Bey, I.; Yantosca, R. M. Constraints from [210] Pb and [7] Be on Wet Deposition and Transport in a Global Three-Dimensional Chemical Tracer Model Driven by Assimilated Meteorological Fields. *J. Geophys. Res.: Atmos.* **2001**, *106*, 12109−12128.

(55) Clarke, L.; Edmonds, J.; Jacoby, H.; Pitcher, H.; Reilly, J.; Richels, R. *Scenarios of Greenhouse Gas Emissions and Atmospheric Concentrations*; U.S. Department of Energy Publications, 2007.

(56) Fujino, J.; Nair, R.; Kainuma, M.; Masui, T.; Matsuoka, Y. Multi-Gas Mitigation Analysis on Stabilization Scenarios Using Aim Global Model. *Energy J.* **2006**, *27*, 343−353.

(57) Riahi, K.; Grübler, A.; Nakicenovic, N. Scenarios of Long-Term Socio-Economic and Environmental Development under Climate Stabilization. *Technol. Forecast. Soc. Change* **2007**, *74*, 887−935.

(58) van Vuuren, D. P.; den Elzen, M. G. J.; Lucas, P. L.; Eickhout, B.; Strengers, B. J.; van Ruijven, B.; Wonink, S.; van Houdt, R. Stabilizing Greenhouse Gas Concentrations at Low Levels: An Assessment of Reduction Strategies and Costs. *Clim. Change* **2007**, *81*, 119−159.

(59) van Vuuren, D. P.; Edmonds, J. A.; Kainuma, M.; Riahi, K.; Weyant, J. A Special Issue on the RCPs. *Clim. Change* **2011**, *109*, 1.

(60) Keller, C. A.; Long, M. S.; Yantosca, R. M.; Da Silva, A. M.; Pawson, S.; Jacob, D. J. HEMCO v1.0: A Versatile, ESMF-Compliant Component for Calculating Emissions in Atmospheric Models. *Geosci. Model Dev.* **2014**, *7*, 1409−1417.

(61) Van Damme, M.; Erisman, J. W.; Clarisse, L.; Dammers, E.; Whitburn, S.; Clerbaux, C.; Dolman, A. J.; Coheur, P.-F. Worldwide Spatiotemporal Atmospheric Ammonia (NH3) Columns Variability Revealed by Satellite. *Geophys. Res. Lett.* **2015**, *42*, 8660−8668.

(62) Ritchie, H.; Roser, M. CO_2 and Greenhouse Gas Emissions. *Our World Data* **2017**.

(63) Röckmann, T.; Kaiser, J.; Crowley, J. N.; Brenninkmeijer, C. A. M.; Crutzen, P. J. The Origin of the Anomalous or "Mass-Independent" Oxygen Isotope Fractionation in Tropospheric N2O. *Geophys. Res. Lett.* **2001**, *28*, 503−506.

(64) Abbatt, J. P. D.; Benz, S.; Cziczo, D. J.; Kanji, Z.; Lohmann, U.; Möhler, O. Solid Ammonium Sulfate Aerosols as Ice Nuclei: A Pathway for Cirrus Cloud Formation. *Science* **2006**, *313*, 1770−1773.

(65) Nault, B. A.; Campuzano-Jost, P.; Day, D. A.; Jo, D. S.; Schroder, J. C.; Allen, H. M.; Bahreini, R.; Bian, H.; Blake, D. R.; Chin, M.; Clegg, S. L.; Colarco, P. R.; Crounse, J. D.; Cubison, M. J.; DeCarlo, P. F.; Dibb, J. E.; Diskin, G. S.; Hodzic, A.; Hu, W.; Katich, J. M.; Kim, M. J.; Kodros, J. K.; Kupc, A.; Lopez-Hilfiker, F. D.; Marais, E. A.; Middlebrook, A. M.; Andrew Neuman, J.; Nowak, J. B.; Palm, B. B.; Paulot, F.; Pierce, J. R.; Schill, G. P.; Scheuer, E.; Thornton, J. A.; Tsigaridis, K.; Wennberg, P. O.; Williamson, C. J.; Jimenez, J. L. Chemical Transport Models Often Underestimate Inorganic Aerosol Acidity in Remote Regions of the Atmosphere. *Commun. Earth Environ.* **2021**, *2*, No. 93.

(66) Guo, H.; Sullivan, A. P.; Campuzano-Jost, P.; Schroder, J. C.; Lopez-Hilfiker, F. D.; Dibb, J. E.; Jimenez, J. L.; Thornton, J. A.; Brown, S. S.; Nenes, A.; Weber, R. J. Fine Particle PH and the Partitioning of Nitric Acid during Winter in the Northeastern United States. *J. Geophys. Res.: Atmos.* **2016**, *121*, 10355−10376.

(67) Jang, M.; Czoschke, N. M.; Lee, S.; Kamens, R. M. Heterogeneous Atmospheric Aerosol Production by Acid-Catalyzed Particle-Phase Reactions. *Science* **2002**, *298*, 814−817.

(68) RCP Database. https://tntcat.iiasa.ac.at/RcpDb/dsd?Action= htmlpage&page=compare (accessed April 9, 2021).

(69) Bryukov, M. G.; Kachanov, A. A.; Timonnen, R.; Seetula, J.; Vandoren, J.; Sarkisov, O. M. Kinetics of HNO Reactions with O2 and HNO. *Chem. Phys. Lett.* **1993**, *208*, 392−398.